Available online at www.sciencedirect.com
SCIENCE DIRECT®
Journal of Magnetic Resonance 168 (2004) 110–117
JMR Journal of Magnetic Resonance
www.elsevier.com/locate/jmr

Tailored sinc pulses for uniform excitation and artifact-free radio frequency time-domain EPR imaging

N. Devasahayam, R. Murugesan,[1] K. Matsumoto, J.B. Mitchell, J.A. Cook, S. Subramanian, and M.C. Krishna*

Radiation Biology Branch, Center for Cancer Research, National Cancer Institute, National Institutes of Health, Bethesda, MD 20892, USA

Received 14 November 2003; revised 26 January 2004

Abstract

A method to generate shaped radiofrequency pulses for uniform excitation of electron spins in time-domain radio frequency (RF) electron paramagnetic resonance (EPR) imaging is presented. A commercial waveform generator was integrated with the transmit arm of the existing time-domain RF-EPR spectrometer to generate tailored excitation pulses with sub-nano second resolution for excitation with a 90° flip-angle. A truncated sinc [$\sin(x)/x$] pulse, tailored to compensate for the Q-profile (RF frequency response) of the resonator, was shown to yield images from phantom objects as well as in vivo images, with minimal distortion. These studies point to the advantages in using shaped sinc pulses to achieve improved uniform excitation over a relatively wide bandwidth region in time-domain RF-EPR imaging (RF-FT-EPRI).
Published by Elsevier Inc.

1. Introduction

Considerable progress in biological applications of low frequency EPR imaging has been achieved during the last few years [1–5]. Many low frequency (1.2 GHz–220 MHz) EPR spectrometers operating in continuous-wave (CW) mode have been developed to detect and image free radicals in vivo [6–11]. In contrast, only a few time-domain RF-EPR spectrometers have been described for imaging applications [12–14]. EPR methods in time-domain has the potential to reduce acquisition times, making image data collection times compatible with the biological half-life of commonly used EPR spin probes. Although the feasibility of Fourier domain EPR imaging has been demonstrated [15–17], the short T_2^* of biologically viable EPR spin probes make Fourier EPR imaging using pulsed field gradients challenging. Therefore, in time-domain EPR imaging, projections are collected in the presence of static magnetic field gradients in a polar grid and images are reconstructed using filtered back projection (FBP) method [18–20]. Being a pure frequency-encoding method, the FBP technique requires accurate phasing of the sampled time-domain magnetization and hence it is prone to artifacts arising from spectrometer dead time in time-domain EPR mode [21]. Obtaining spectroscopic information by EPRI is of prime importance in biological applications such as pharmacokinetics, in vivo oximetry, etc. [22,23]. For reliable interpretation of EPRI data, image data collection with minimal distortion should be ensured. We have recently reported the use of a pure phase encoding technique called single point imaging (SPI), to circumvent artifacts associated with the FBP method in the time-domain EPR imaging [24,25]. Nevertheless, the excitation pulse shapes as well as the Q-profiles of the large bandwidth resonators required for imaging large size objects may lead to distortions in image quality when using SPI. By Q-profile, we refer to the profile of the actual excitation power density, which has typically a Lorentzian shape centered around the carrier frequency, with the width at 3 dB point from the peak being inversely related to the quality factor Q of the coil. In time-domain EPR imaging, where the bandwidths greater than 10 MHz are required for small animal imaging, the Q-profile of the coil can lead to

* Corresponding author. Fax: 1-301-480-2238.
E-mail address: murali@helix.nih.gov (M.C. Krishna).
[1] On leave from Madurai Kamaraj University, Madurai, India.

1090-7807/$ - see front matter. Published by Elsevier Inc.
doi:10.1016/j.jmr.2004.01.016

distinctively attenuated image intensities at the extremes. Such distortions have been observed in EPR spectra of nitroxides obtained in time-domain and the possibility of using tailored pulses for uniform spectral excitation has been indicated [26–28]. In this report the use of shaped pulses to obtain uniform excitation across the entire object as well as to minimize Q-profile artifacts in time-domain RF-EPR images was examined.

2. Excitation pulse profile

In our earlier pulsed RF-EPR imaging studies, a conventional rectangular pulse (the so-called hard pulse) was used to excite the spins in the presence of a static magnetic field gradient [18–21,23–25]. The Fourier transform of the rectangular pulse has the characteristic sinc-shaped $[\sin(x)/x]$ excitation profile. This may not be optimal for imaging applications, because it introduces 'sinc-like' side lobes symmetric about the central frequency of excitation, which get progressively weaker with resonance offset. For a pulse width t_p, the central lobe, which zero-crosses at frequencies $\pm 1/2t_p$, is centered on the carrier frequency, and uniform excitation is possible only for half this range. With such a profile, the excitation becomes non-uniform and the resulting sensitivity loss, especially in the outer regions of the images can be significant. One useful frequency-domain excitation profile can be a rectangular pulse (sometimes called the 'top-hat' shape) with abrupt transitions from full to negligible excitation at the edges and uniform excitation in between. Shaped pulses of short-duration may help to achieve more uniform excitation profiles over the extended frequency ranges often needed for EPR imaging applications. Of the various types of excitation schemes for uniform excitation, the sinc pulse is easy to implement. The sinc pulse represents the inverse Fourier transform of a rectangular profile and, therefore, should produce a uniform excitation profile. The advantage of sinc pulse over a rectangular pulse is that the former essentially exchanges power in the center of the excitation band for power at the edges.

3. Pulse shaping for Q-profile compensation

As previously mentioned, the transient magnetization resulting from a spin system by irradiating with a rectangular RF pulse is not flat across the spectral bandwidth and hence the observed image intensity can be distorted. This artifact is further compounded by the Q-profile of the resonator. The Q-profile of the resonator has a characteristic Lorentzian shape with progressively reduced amplitude towards either extreme of the frequency bandwidth. Use of shaped pulses for slice selection and selective uniform excitation in MRI and MRS is well established [29–32]. But the selective pulses used in MRI/MRS need to cover relatively small bandwidths (10–20 kHz). Because of the low bandwidth requirements, Q-profile artifacts are negligible in MRI. Unlike in MRI, the bandwidth required for EPR imaging of even a small animal (such as mouse with a moderate space encoding gradient of about 1 G/cm) is large (approximately 12 MHz). Such a large bandwidth places restrictions on the selection of image acquisition parameters such as the quality factor Q of the resonator, the pulse width, pulse shape, pulse power etc. One can use pulse shaping, (Gaussian, sinc, and tailored pulses) to correct for the Q-profile artifacts. Fig. 1 shows the relationship between the pulse profile, and the corresponding power spectrum (spectral profile), which are related by Fourier transform of each other. In the figure, the left column shows (A) rectangular pulse, (B) a sinc pulse, (C) a truncated sinc pulse with only one side lobe on either side, (D) same as in (C) but with the side lobes scaled down by a factor of 2 and, (E) same as in (C) but with the side lobes scaled up by a factor of 2. The corresponding spectral density profiles are shown in the right column (P, Q, R, S, and T). Only the region corresponding to the central lobe and two side lobes of the power spectrum corresponding to the rectangular pulse (P) is shown in the left column. The ideal sinc pulse, with all the lobes taken into account, gives the ideal rectangular (top-hat) spectral profile (Q), but this is not practical, since the pulse length required will be too long (>500 ns) for time-domain EPR. The sinc pulse with just a single side lobe on either side provides a reasonably flat power spectrum, but the truncation has created a dip in the middle of the profile (R). If one scales down the side lobes relative to the central lobe (here by a factor of 2), the central dip in the power spectrum can be removed (S), but the profile becomes trapezoidal with a slightly slanted rise and fall at the edges. Such a power spectrum may be adequate for imaging and can produce the required uniform excitation, if the coil response in the frequency range of interest is flat. Unfortunately, because of the finite Q factor of the coil, albeit quite small in time-domain EPR (around 25 at 300 MHz), there will be considerable power droop on either extreme. If the side lobes are scaled up by a factor greater than one (here by a factor of 2), a noticeable increase in the power density at the extremes can be realized compared to the center (T), and one can appropriately scale the relative amplitudes of the central to side lobes to compensate for the drop in power at the extremes brought about by the coil Q. In summary, a sinc pulse with a side lobe on either side, with the relative intensities of the central lobe to side lobe suitably scaled, should compensate for the Q profile characteristics and provide uniform excitation throughout the sample.

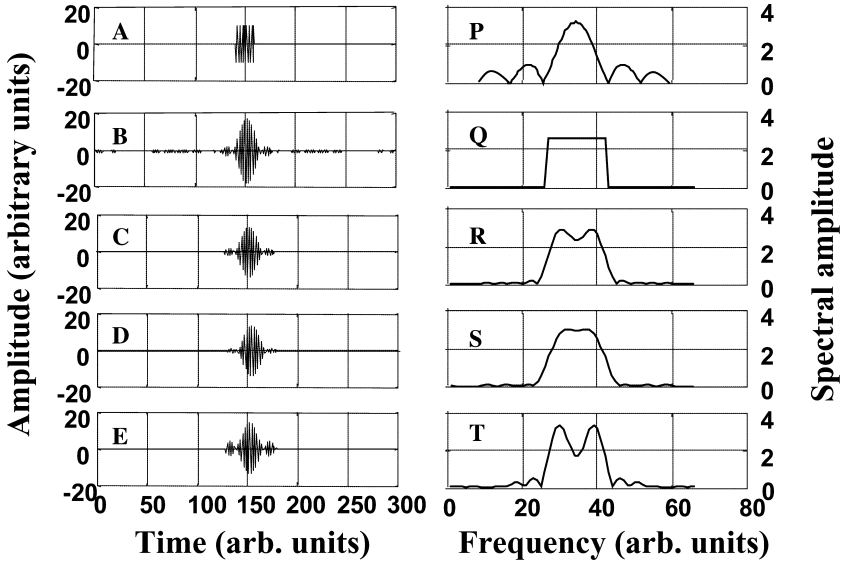

Fig. 1. Fourier Relationship between pulse shape and the corresponding power spectrum. In the left columns, A, B, C, D, and E corresponds, respectively, to a rectangular, ideal sinc, truncated sinc with only one side lobe on either side, side-lobe-attenuated sinc and side-lobe-enhanced sinc pulses. In the right column, the corresponding power spectra close to the carrier frequency are shown. The rectangular pulse generates the sinc profile power spectrum (P) while the sinc pulse generates the ideal uniform excitation (Q). The truncated sinc pulse of width t shows more uniform excitation in the frequency region $\pm 1/2t$ centered on the carrier compared to the rectangular pulse, but it has a slight concave power profile at the center (R). This can be made more uniform by reducing the intensity of the side lobe relative to the central lobe (S). An enhancement of the side lobe intensity leads to an increase of spectral density at the extremes of the power profile with a concomitant reduction in the center (T), and thus can compensate for the coil Q-profile.

4. Generation of shaped pulses

Shaped radio frequency pulses are generated on modern high-resolution spectrometers by means of a digitally controlled waveform generator that feeds the custom designed waveform to a linear radiofrequency power amplifier [33]. Compared to MRI, pulsed EPRI needs very high time resolution (<1 ns) because of the very short excitation pulses (70–110 ns) used [34].

The sinc pulse can be generated by using shaped-pulse hardware or by a series of attenuated hard pulses. The pulse shape can be calculated by the minimum size attainable by the hardware in order to achieve finest possible digital time resolution. The pulse length can be calculated from known square-pulse parameters for the same power level and the relative integrated power of the sinc pulse using the equation

$$t_{\text{sinc}} = t_{\text{hard}} \times P_{\text{hard}}/P_{\text{sinc}}. \quad (1)$$

Here, t_{sinc} and t_{hard} are the pulse lengths and P_{hard} and P_{sinc} are the power levels for the sinc and hard pulse, respectively. But, because a true sinc function has extensive (oscillatory) wings, and because the pulse duration must be minimized, it is useful to truncate the sinc function at one of the zero-crossing points (often second or third). A truncated sinc pulse is a common RF pulse used to obtain an approximately rectangular slice selection profile in MRI (Fig. 1).

5. Experimental

A commercial waveform generator, ANALOGIC DBS 2050A (Analogic, Peabody, MA) was selected based on its sampling rate (2.4 Gs/s, single channel) as well as its capability to generate precise standard waveforms (square, sine, positive and negative ramps, sinc, etc.). Very short rise/fall times of the pulses (400 ps), good vertical resolution (8 bits) and high programmable gain (60 dB) and offset are other added advantages provided by the ANALOGIC DBS 2050A. In addition, the instrument comes in VXI Chassis with 'Plug and Play' compliant software drivers. Fig. 2 presents the schematics describing the integration of the pulse shaping unit with the transmit arm of the pulsed RF FT EPR imager. This block diagram includes the modifications made to accommodate the arbitrary waveform generator DBS 2050A. All the timing and gated modules are phase locked to a master oscillator of 800 MHz. The output of the master oscillator is fed to a frequency synthesizer to generate 5, 10, 20, 50, 100, 200, and 400 MHz signals, which are phase-locked to the 800 MHz master frequency. The 10 MHz signal is used as the external clock and 5 MHz signal is used as the external trigger input for the DG535 delay pulse generators. Of the three daisy-chained DG535 delay generators, the first one provides the timing signal for the repetition rate. All other timing pulses required for the time-domain EPR

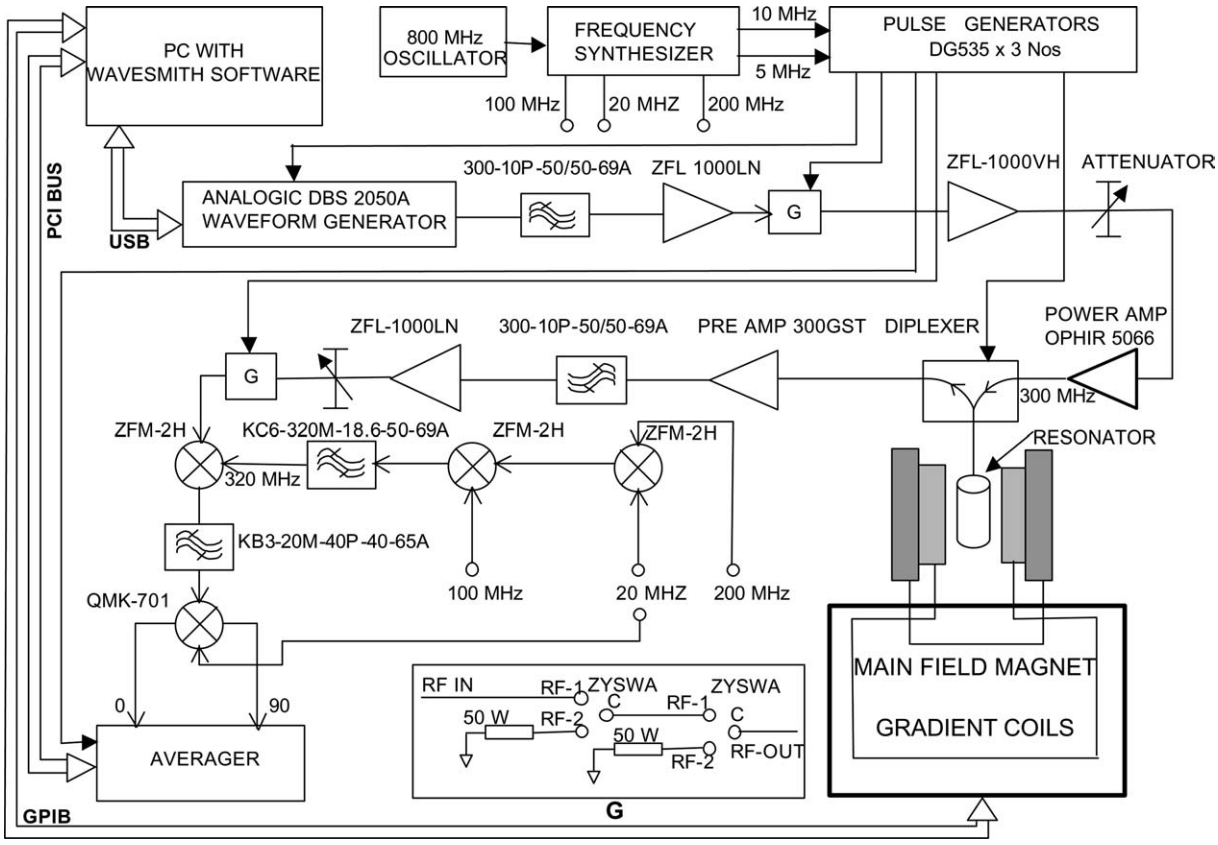

Fig. 2. Schematics of the pulsed RF-EPR spectrometer/imager showing the integration of the waveform generator with the transmit arm of the spectrometer.

imager, including the waveform generator, are referenced to this signal.

The other signals (20, 100, and 200 MHz) are used in the mixer as well as in the demodulating circuits as shown in Fig. 2. The quadrature outputs, I and Q are generated first by down converting the 300 MHz signal to 20 MHz by mixing it with 320 MHz. The 20 MHz output signal is fed to a demodulator (QMK-701, Synergy Microwave, NJ 07504) along with a reference (20 MHz) to obtain I and Q outputs. The direct conversion of the 300 MHz EPR signals to base band is avoided to eliminate the system feed through. This is because, if we had the 300 MHz signal persistent during acquisition, due to the high amplification of the EPR signals nearly by 60 dB, there will be considerable feed through of the signal, leading to unacceptable levels at zero-frequency during conversion to base band.

Using the Wavesmith waveform development system, application software supplied along with the arbitrary waveform generator, the required waveforms were generated. A draw or sketch option is also available to "custom design" a particular wave shape. For imaging applications, rectangular and sinc pulses were generated and used to modulate the carrier frequency (300 MHz), which was also generated by the waveform generator. Fig. 3A shows these waveforms and the modulated 300 MHz carrier. The discrete waveforms with sub nanosecond digital resolution (sampling frequency, 2.4 GHz) becomes continuous on passing through a band pass filter (300 MHz, type KC6- 300-10P-50/50-69A, TTE Incorporated, Los Angeles, CA). The output from the arbitrary waveform generator was adjusted to −3 dB, filtered and finally fed to an RF amplifier (ZFL-1000LN, Mini-Circuits, Branson, MO 65615) to obtain the excitation pulse.

6. Mapping of power spectral profiles

In order to map the actual power spectral profiles, a point sample of TCNQ (*N*-methylpyridinium tetracyanoquinonedimethane) crystals is placed in a capillary tube at the center of a 25 mm × 25 mm parallel coil resonator [19] tuned to 300 MHz with a Quality factor of ≈ 25. TCNQ gives a strong exchange narrowed single line at $g = 2.0$. Rectangular pulses of duration 70 and 110 ns, and tailored sinc pulses with one lobe on either side with the central lobe duration of 70 and 110 ns were used, after amplifying the same to 200 W using a linear power amplifier (Model 5006, Ophir RF, Los Angeles, CA 90066). The transmitter and the receiver were isolated using a diplexer [12] as shown in Fig. 2.

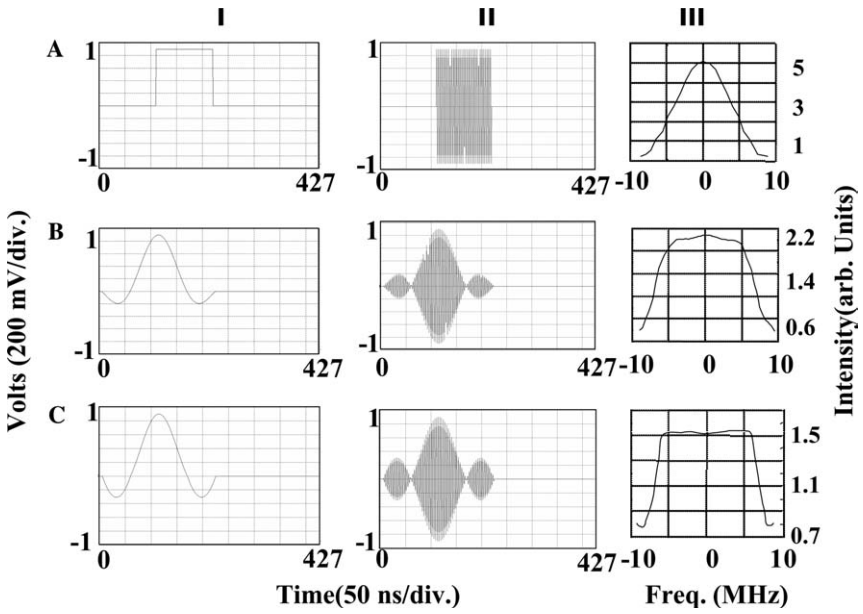

Fig. 3. Pulse shape (I), modulated carrier (II), and the corresponding (measured) excitation profile of the resonator (III) for: (A) square pulse, (B) truncated sinc pulse, and (C) tailored sinc pulse for Q-compensation. The power spectral profiles were mapped as explained in the text.

EPR induction signals were amplified and down-converted to base band, and were detected in quadrature. The signals were acquired using a fast digitizer (Model AP100, Acquiris USA, Monroe, CA 10950) at 500 Ms/s. A total of 20,000 responses were averaged per spectrum, and the resulting FID was Fourier transformed and the signal heights were measured in the magnitude mode. The power spectral profile was mapped by monitoring the peak amplitude of the spectrum, by changing the magnetic field in small steps in such a way that the resonance frequency covered an offset of −9 to +9 MHz. The peak intensity was plotted as a function of offset frequency from the center to produce the spectral density profile.

7. EPR imaging

EPR imaging was carried out on a phantom consisting of four tubes (4-mm id) filled with identical number of spins in a volume of 45 μL of 5 mM solution of Oxo63 [19], arranged axially along a 25 mm × 50 mm parallel coil resonator. The relationship between Q of the resonator and pulse width (t_p) is approximately given by [35]

$$Q = \omega_0 t_p/4, \tag{2}$$

where ω_0 is the frequency of operation, t_p is the pulse duration. This criterion leads to a Q value of 52 for a pulse width of 110 ns. However, in practice Q values have been deliberately chosen to be less than that allowed by the above equation in order to reduce the ringing time and provide the necessary bandwidth ~12 MHz. Hence Q was chosen to be 25 in the present study. Two-dimensional cross sectional RF-FT-EPR images were obtained using the single point imaging (SPI) technique, a pure phase encoding method, the experimental details of which are similar to those reported earlier [23]. A maximum gradient of 0.8 G/cm, and a field of view of 60 mm, corresponding to a frequency spread of about 13 MHz were selected for imaging. The number of phase encoding steps was 21 along the long axis and 11 along the short axis of the field of view. A single point at 500 ns from the trailing edge of the pulse was chosen for image reconstruction.

8. Results and discussion

Fig. 3 summarizes the results of power profile measurements. The column I shows the pulse profiles (rectangular, sinc and modified sinc) and column II the corresponding pulses at 300 MHz and column III the experimentally determined (as described earlier) excitation profiles of the various pulse shapes. Maximum available linear peak power was applied in all the cases. Truncated sinc pulses were used to minimize the pulse length so that the dead time can be kept as short as possible. The B_1 profile of the truncated sinc pulse is given by

$$B_1(t) \propto \mathrm{sinc}(2t/p), 0 = |t| = np/2; \quad B_1(t) = 0, |t| > np/2, \tag{3}$$

where $\mathrm{sinc}(x) = \sin(\pi x)/\pi x$. It could be readily seen from Fig. 3 that the truncated sinc pulse generates a uniform excitation profile over the desired bandwidth.

Its efficiency remains uniform across the entire bandwidth while the efficiency of the hard pulse declines in regions away from the transmitter center frequency. Small oscillations observed at the edges of the power profile from the sinc pulse (not shown), are due to truncation of the ideal sinc pulse beyond the first side lobe. The sinc pulse can be Hamming-windowed to reduce the Gibbs ringing at the edges, but no such attempt was made in our studies. The profile of the tailored sinc pulse (by adjusting the amplitude of the side lobes relative to the central lobe) shows enhanced RF flux at the extremes and can correct for the Q-profile.

To examine the effects of shaped pulses on image profiles, EPR imaging experiments were carried out in the SPI mode. Results of imaging of a four-tube phantom are summarized in Fig. 4. Image intensity as a function of distance from the center shows symmetrical reduction, although the spin content was the same in all the four tubes. Images obtained with the 110 ns rectangular pulse show that intensity of the outer tubes are less than the inner ones. The attenuation of the intensities of the outer tubes is caused by both the nature of the spectral excitation profile as well as the Q-profile of the resonator. This can lead to errors in the quantitative measurement of spin concentration from the observed image intensities. Fig. 4A shows the image obtained for the four-tube phantom (each tube containing the same number of spins) and one can clearly see the effect of the power spectral profile, compounded by the resonator Q-profile. A 70 ns rectangular pulse improved the uniformity in excitation a little better than the one obtained with 110 ns rectangular pulse (data not shown). A regular sinc pulse with a single side lobe on either side shows some improvement in the intensity variation (data not shown). Nevertheless, intensities of the outer tubes were still lower than those of the inner tubes. Images obtained with the tailored sinc pulses (Fig. 4B), on the other hand, show that intensities of all the four tubes are practically the same. Thus the Q-compensated tailored

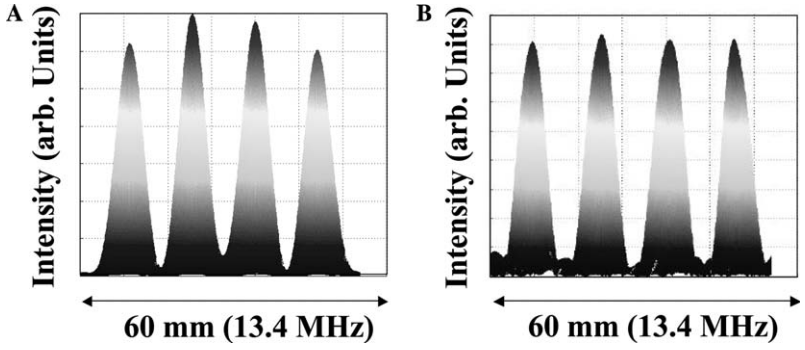

Fig. 4. 2D mesh plots, 2D projection images of the four-tube phantom (all the four tubes, 4 mm i.d., contained equal spin count, 45 μL of 5 mM Oxo63) and the profile of the resonator power spectrum for (A) rectangular pulse: 110 ns. (B) Tailored sinc pulse: overall length 130 ns. The flattening of the power spectrum in going from rectangular to sinc profile and the equalization of intensities in the mesh plots can be clearly seen.

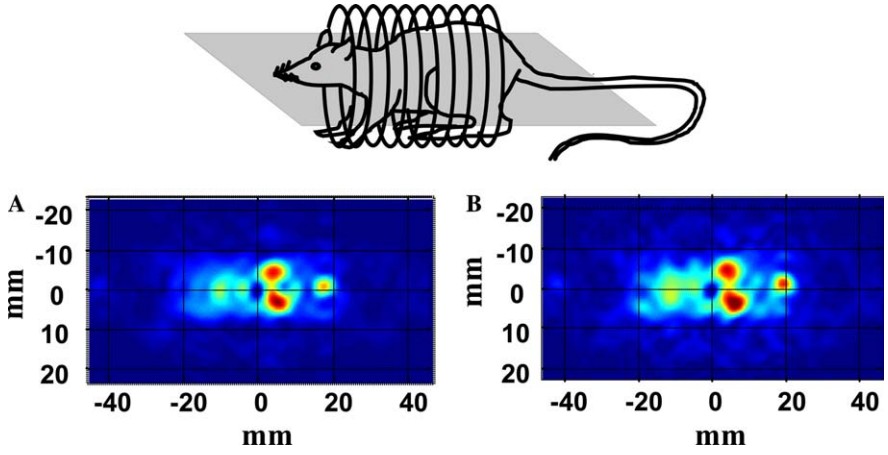

Fig. 5. 2D images of C3H mouse obtained using a 110 ns (A) rectangular and (B) modified sinc pulse in a 25 × 50 mm cylindrical resonator with a Q of 25. Images taken with a rectangular pulse show marked decrease in intensity at the periphery of the image. A cartoon of the mouse in the resonator coil and the image plane is shown on the top (not to scale). Note that there is no slice selection possible, and the overall spin distribution is projected on the image plane.

sinc pulse is effective in minimizing the intensity distortion in FT EPR imaging. However, since the integrated power of the truncated sinc pulse is less than that of the square pulse (Fig. 3C), the intensities of images generated using sinc pulses are lower than those generated by hard pulses of identical pulse height. Since the same power amplifier with its maximum output was used for both the experiments, generating a 90° sinc pulse was not possible.

We have also evaluated the use of tailored sinc pulse for in vivo applications. Fig. 5 shows 2D images of a C3H mouse infused with 75 μL of 100 mM Oxo63 solution obtained with a 90° rectangular pulse (A), and a tailored sinc pulse that provides a uniform excitation with additional compensation for the Q-profile of the resonator (B). It can be seen that the rectangular pulse provides a relatively intense central region with a reduced intensity for the bladder and thoracic region, whereas, the tailored pulse achieves a more uniform excitation bringing in extra details from the extreme regions of the field of view as evidenced by improved intensity of the bladder and more details in the thoracic region. The tailored pulse, thus provides relatively uniform excitation throughout the entire bandwidth corresponding to the filed of view.

9. Conclusion

In pulsed RF-EPRI, a 90° rectangular pulse is used for the excitation of the spins. Such a hard pulse leads to artifacts in images because of its non-uniform excitation profile across the sample. In addition, the Q-profile of the large bandwidth low Q resonator can also distort the EPR images. In smaller objects or low resolution imaging applications, where the gradient values are low, such distortions are not too evident. But, as the bandwidth requirement increases, this effect can be quite significant. It can distort the image and also can lead to errors in quantitative parameter estimation. In this paper, three different waveforms were used and their experimental excitation profiles were determined. It is shown that using a tailored sinc pulse, excitation as well as the resonator Q-profile artifacts in pulsed RF-EPRI can be readily corrected.

References

[1] B.B. Williams, H. Al Hallaq, G.V.R. Chandramouli, E.D. Barth, J.N. Rivers, M. Lewis, V.E. Galtsev, G.S. Karczmar, H.J. Halpern, Imaging spin probe distribution in the tumor of a living mouse with 250 MHz EPR: correlation with BOLD MRI, Magn. Reson. Med. 47 (2002) 634–638.
[2] H.M. Swartz, T. Walczak, Developing in vivo EPR oximetry for clinical use, Adv. Exp. Med. Biol. 454 (1998) 243–252.
[3] H. Sano, M. Naruse, K. Matsumoto, T. Oi, H. Utsumi, A new nitroxyl-probe with high retention in the brain and its application for brain imaging, Free Radic. Biol. Med. 28 (2000) 959–969.
[4] P. Kuppusamy, R.A. Shankar, V.M. Roubaud, J.L. Zweier, Whole body detection and imaging of nitric oxide generation in mice following cardiopulmonary arrest: detection of intrinsic nitrosoheme complexes, Magn. Reson. Med. 45 (2001) 700–707.
[5] M.C. Krishna, D. Devasahayam, J.A. Cook, S. Subramanian, P. Kuppusamy, J.B. Mitchell, Electron paramagnetic resonance for small animal imaging, ILAR J. 42 (2001) 209–218.
[6] J.A. Brivati, A.D. Stevens, M.C.R. Symons, A radiofrequency ESR spectrometer for in vivo imaging, J. Magn. Reson. 92 (1991) 480–489.
[7] D. Dijret, M. Beranger, A. Bernerd, C. Jeandey, M. Moussavi, A new 280-MHz ESR spectrometer, J. Chim. Phys. PCB. 91 (1994) 1862–1867.
[8] H.J. Halpern, D.P. Spencer, J. van Polen, M.K. Bowman, A.C. Nelson, E.M. Dowey, B.A. Teicher, Imaging radio frequency electron-spin-resonance spectrometer with high resolution and sensitivity for in vivo measurements, Rev. Sci. Instrum. 60 (1989) 1040–1050.
[9] M. Alecci, S. Dellapenna, A. Sotgui, L. Testa, I. Vannucci, Electron-paramagnetic resonance spectrometer for 3-dimensional invivo imaging at very low-frequency, Rev. Sci. Instrum. 63 (1992) 4263–4270.
[10] A.D. Stevens, J.A. Brivati, A 250 MHz Epr spectrometer with rapid phase-error correction for imaging large biological specimens, Meas. Sci. Technol. 5 (1994) 793–796.
[11] J. Koscielniak, N. Devasahayam, M.S. Moni, P. Kuppusamy, K. Yamada, J.B. Mitchell, M.C. Krishna, S. Subramanian, 300 MHz continuous wave electron paramagnetic resonance spectrometer for small animal in vivo imaging, Rev. Sci. Instrum. 71 (2000) 4273–4281.
[12] R. Murugesan, M. Afeworki, J.A. Cook, N. Devasahayam, R. Tschudin, J.B. Mitchell, S. Subramanian, M.C. Krishna, A broadband pulsed radio frequency electron paramagnetic resonance spectrometer for biological applications, Rev. Sci. Instrum. 69 (1998) 1869–1876.
[13] M. Alecci, J.A. Brivati, G. Placidi, A. Sotgiu, A radiofrequency (220-MHz) Fourier transform EPR spectrometer, J. Magn. Reson. 130 (1998) 272–280.
[14] R.W. Quine, G.W. Rinard, S.S. Eaton, G.R. Eaton, A pulsed and continuous wave 250 MHz electron paramagnetic resonance spectrometer, Conc. Magn. Reson. (Magn. Reson. Engineer.) 15 (2002) 59–91.
[15] A. Feintuch, G. Wlexandrowicz, T. Tashma, Y. Boasson, A. Grayevsky, N. Kaplan, Three-dimensional pulsed ESR Fourier imaging, J. Magn. Reson. 142 (2000) 382–385.
[16] A. Coy, N. Kaplan, P.T. Callaghan, Three-dimensional pulsed ESR imaging, J. Magn. Reson. A 121 (1996) 201–205.
[17] U. Ewert, R.H. Crepeau, C.R. Dunnam, D.J. Xu, S.Y. Lee, J.H. Freed, Fourier-transform electron-spin-resonance imaging, Chem. Phys. Lett. 184 (1991) 25–33.
[18] R. Murugesan, J.A. Cook, N. Devasahayam, M. Afeworki, S. Subramanian, R. Tschudin, J.A. Larsen, J.B. Mitchell, A. Russo, M.C. Krishna, In vivo imaging of a stable paramagnetic probe by pulsed-radiofrequency electron paramagnetic resonance spectroscopy, Magn. Reson. Med. 38 (1997) 409–414.
[19] M. Afeworki, G.M. van Dam, N. Devasahayam, R. Murugesan, J. Cook, D. Coffin, J.H. Larsen, J.B. Mitchell, S. Subramanian, M.C. Krishna, Three-dimensional whole body imaging of spin probes in mice by time-domain radiofrequency electron paramagnetic resonance, Magn. Reson. Med. 43 (2000) 375–382.
[20] N. Devasahayam, S. Subramanian, R. Murugesan, J.A. Cook, M. Afeworki, R.G. Tschudin, J.B. Mitchell, M.C. Krishna, Parallel coil resonators for time-domain radiofrequency electron

paramagnetic resonance imaging of biological objects, J. Magn. Reson. 142 (2000) 168–176.
[21] K.I. Yamada, R. Murugesan, N. Devasahayam, J.A. Cook, J.B. Mitchell, S. Subramanian, M.C. Krishna, Evaluation and comparison of pulsed and continuous wave radiofrequency electron paramagnetic resonance techniques for in vivo detection and imaging of free radicals, J. Magn. Reson. 154 (2002) 287–297.
[22] B. Gallez, G. Bacic, F. Goda, J.J. Jiang, J.A. OHara, J.F. Dunn, H.M. Swartz, Use of nitroxides for assessing perfusion, oxygenation, and viability of tissues: in vivo EPR and MRI studies, Magn. Reson. Med. 35 (1996) 97–106.
[23] S. Subramanian, K. Yamada, A. Irie, R. Murugesan, J.A. Cook, N. Devasahayam, G.M. Van Dam, J.B. Mitchell, M.C. Krishna, Noninvasive in vivo oximetric imaging by radiofrequency FT EPR, Magn. Reson. Med. 47 (2002) 1001–1008.
[24] S. Subramanian, N. Devasahayam, R. Murugesan, K. Yamada, J. Cook, A. Taube, J.B. Mitchell, J.A.B. Lohman, M.C. Krishna, Single-point (constant-time) imaging in radiofrequency Fourier transform electron paramagnetic resonance, Magn. Reson. Med. 48 (2002) 370–379.
[25] A.G. Taube, S. Subramanian, R. Murugesan, N. Devasahayam, J.B. Mitchell, M.C. Krishna, J.A. Cook, An application system for automation of constant-time radiofrequency electron paramagnetic resonance imaging, Comput. Methods Programs Biomed. 72 (2003) 127–138.
[26] J. Gorcester, J.H. Freed, Two-dimensional Fourier transform electron spin resonance correlation spectroscopy, J. Chem. Phys. 88 (1988) 4678–4693.
[27] P.P. Borbat, R.H. Crepeau, J.H. Freed, Multifrequency two-dimensional Fourier transform ESR: an X/Ku-band spectrometer, J. Magn. Reson. 127 (1997) 155–167.
[28] J.P. Hornak, J.H. Freed, Spectral rotation in pulsed ESR spectroscopy, J. Magn. Reson. 67 (1986) 501–518.
[29] R. Freeman, Shaped radiofrequency pulses in high resolution NMR, in: J. W. Emsley, J. Feeney, L. H. Sutcliffe (Series Eds.), Progress in Nuclear Magnetic Resonance Spectroscopy, Pergamon, Oxford, 1998.
[30] J.M. Pope, D. Jonas, R.R. Walker, Choice of soft pulse shapes for signal excitation in chemical shift selective imaging, Magn. Reson. Imaging 13 (1995) 763–766.
[31] D.E. Hyre, L.D. Spicer, Improved excitation pulse bandwidths using shaped pulses, with application to heteronuclear half filters in macro molecular NMR, J. Magn. Reson. 108 (1995) 12–21.
[32] D.J. Lurie, A systematic design procedure for selective pulses in NMR imaging, Magn. Reson. Imaging 3 (1985) 235–243.
[33] J.A.J. Temps, Synthesis of arbitrary frequency domain transmitting pulses applicable to pulsed NMR instruments, J. Magn. Reson. 56 (1984) 335–372.
[34] R.W. Quine, J.R. Harbridge, S.S. Eaton, G.R. Eaton, Design of a programmable timing unit, Rev. Sci. Instrum. 70 (1999) 4422–4432.
[35] W.B. Mims, Electron spin echoes, in: S. Geschwind (Ed.), Electron Paramagnetic Resonance, Plenum Press, New York, 1972 pp. 263–351.